Novel Planar Continuum Robot with Spiral Pulley Actuation and Gear Synced Body

Damoon Mohamadi[1], Tatiana Minav[1] and Roel Pieters[1]

***Abstract*—Continuum robots are an attractive solution for navigation in complex and restrictive environments. However, with the existing technology, only two approaches are possible for development of high dexterity continuum robots with low compliance: (i) utilizing a fully articulated body with high number of individually actuated rigid links; (ii) employing a body consisting of flexible sections and strong spring elements. While the former requires numerous actuators, thus a heavy and expensive actuator-pack, the latter necessitates larger and costlier actuators to overcome the spring force. Moreover, the latter approach cannot achieve as low compliance due to its flexible nature. This paper introduces a novel planar continuum robot design that benefits from a fully articulated body divided into individually actuated sections of synchronized links. The kinematic modelling and motion planning of the robot arm are presented and utilized for evaluation of the proposed design. A six-section prototype, consisting of 30 links, validates the proposed designs and demonstrates its performance in both simulation and real experiments on four different paths. The validation is based on distal deviation of individual links from the intended paths. Evaluation verifies that the concepts lead to lower compliance, higher dexterity and actuator-pack size reduction (i.e. one actuator per section), as compared to existing approaches.**

I. Introduction

Continuum robots, also known as snake-arm robots, are proving to be beneficial as compared to manual procedures. The ability to reach confined areas cause their utilization to improve minimally invasive surgeries [1]–[7] as well as in *In situ* inspection and maintenance of various types of machinery. While the former reduces damage to the human body, thus shortening the recovery time of the patients, the latter significantly decreases the corresponding cost and down-time of machinery by eliminating the need for comprehensive disassembly procedures [8]–[11]. In addition, studies have also been carried out to investigate the application of these arms for production automation where reaching closed spaces is required, e.g., inside an airplane wing [12].

As continuum robots commonly are composed of several independently actuated serially linked units, this enables them to move inside constrained environments flexibly. In addition, continuum robots are anchored to their base which, in most cases, is also their source of actuation. The combination of base and arm movements enables their unique abilities for the mentioned applications. In Fig. 1, the prototype built for the purpose of this study is depicted, which includes these two main components, i.e., base (or actuator pack) and arm. Following, this introduction reviews the main characteristics of continuum robots, identifies the technological gaps this study aims to address and finally, presents the proposed solutions.

[1]Cognitive Robotics group, Unit of Automation Technology and Mechanical Engineering, Tampere University, 33720, Tampere, Finland; firstname.surname@tuni.fi

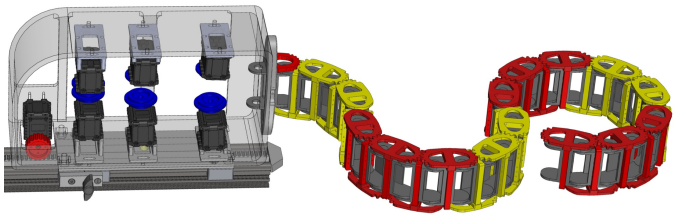

Fig. 1: 3D model of the continuum robot (six sections, 30 links) with actuator pack. Six motors actuate the tendon-based continuum arm, one motor forwards the whole robot and actuator pack. Note: tendons are not shown in the figure.

A. Degrees of Freedom

Continuum robots can be described as a number of serially connected links via joints which, regardless of the joint design, can have either one, two or three degrees of freedom (DoF). Robots consisting of 1 DoF joints can move only in 2D Cartesian space, the ones with 2 or 3 DoF joints can move in 3D Cartesian space while the latter can also change in length [13]. While extra DoF usually means added flexible capabilities, it causes a considerable amount of complexity in terms of mechanical design, control and reliability. Therefore, in the majority of applications, best results are gained when the least necessary DoF are utilized. A competent example of this practice is the work of Wang et al. that presents a 10-section planar arm with a 3-section 2D tip for *In situ* aeroengine inspection and repair [9].

B. Actuation

Actuation of a continuum robot is particularly challenging since the diameter to length ratio is usually significantly small. Thus, a minor force at the end of the arm results in large torques at joints closer to the base. These torques require countering with actuation forces whose affecting points cannot be far from the center due to the relatively narrow diameter. This is mainly the reason that the actuators, minuscule enough to fit inside the arm itself, usually cannot provide the required force. Consequently, the majority of continuum robots have an external actuator pack that houses the actuators strong enough for the application. The major actuation methods utilized in continuum robot arms are summarized as follows.

Tendon driven robots are actuated by a number of tendons pulled by the actuator-pack causing the desired torque and consequently movement at the corresponding joint. Tendons work against each other to ensure the desired movement and shape of the robot. A tendon, regardless of the material, is a rope or wire resembling component with the main duty of bearing tensional stress and is not subject to compression and buckling. This requirement causes a variety of materials and components to be suitable for this purpose. Furthermore, the available tendons can transfer high actuation forces relative to the small volume they occupy within the arm, and the low mass they add to the robot. A study of their mechanics is done by Gonthina et al. [14]

Pneumatically actuated robots have multiple muscle like peripheral chambers that inflate in order to bend the section to the opposite direction. OctArm [15], Festo's BHA [16] and Stiff-Flop [17] are examples of this type. These muscles pose considerable limitation to the design of the robot since they are large in volume and unable to provide high forces, due to usage of a compressible fluid, such as air. For the same reason they fail to provide solid, continuously and precisely controllable actuation.

Hybrid actuated robots use one of the above mentioned methods to move the robot while the other method is used to stiffen it when needed; e.g. tendon based stiffening in the work of Shiva et al. [18]. In this example pneumatic chambers are utilized as actuation source and work against tendons that moderate the stiffness of the arm. Another example is pneumatic layer jamming by Kim et al. [19], which combines tendon actuation with specially designed joints that lock in place due to a pneumatic vacuum.

C. Body Structure

Low diameter to length ratio is a necessity for robot arms aimed to operate in constrained environments. Moreover, a continuum robot body needs to provide high degrees of freedom to achieve the mentioned goal. Multiple design approaches can achieve a flexible or semi-flexible hyper-redundant long robotic arm and the major categories are as follows:

Rigid articulated units have no flexible parts rather only rigid links which are actuated individually. They provide low compliance and kinematic certainty at the expense of mechanical flexibility. For example, OC Robotics Series II - X125, was mounted on a Kuka arm and investigated for aircraft assembly in the work of Buckingham et al. [12].

Flexible sections, e.g. the single section designed by Hu et al. [20] or the one Du et al. used in their work [21], are another approach to provide dexterity for continuum robots. Another variation of this approach is evident in robots with multiple rigid links in each section giving the section semi-flexible properties, e.g., as in the works of Li et al. [22] and Qi et al. [23]. In the latter approach, a spring element, i.e., a flexible backbone, is employed to homogenize the amount of links' movements within a section or the sections are flexible themselves in order to produce the same result.

D. Contributions

Continuum robots require high-strength actuators to achieve precise motion. In case low compliance is needed, i.e., reliable body shape control, only two approaches can be taken based on the current body technology: 1. fully articulated body with high number of body links and 2. flexible sections with strong spring elements. The former approach needs many actuators while the latter needs strong actuators.

This study aims to address these both issues: reducing the actuator pack size of a continuum robot with high kinematic certainty, i.e., low compliance. Therefore, a novel body is proposed that utilizes multi-link, i.e. articulated, sections to achieve high dexterity while the links' movements within each section are homogenized via synchronizing gears. The approach eliminates the need for spring elements while reducing body shape compliance compared to existing technologies. In addition, a novel actuation design is proposed that only requires a single actuator per actuated unit. In the majority of tendon driven planar continuum robot designs, each actuated unit requires two actuators pulling one tendon each that work against each other. As, for a given movement, the amount of required length change in the opposing tendons of the same section are not equal. A special double spiral pulley is designed that collects/releases a pair of tendons unequally and with the correct amount.

To summarize, the contributions of this work are:

- Novel planar tendon driven continuum robot design with gear synced body
- High dexterity of the robot is achieved by articulated sections (five links per section)
- Single actuator per section by double spiral pulley design
- Proof of concept prototype with six sections (30 links) demonstrating accurate path following on high curvature paths

The paper is organized as follows: Section I briefly covers the continuum robots' main applications and explains the most common technologies in the field. Following, two limitations are identified with possible areas for improvement, i.e., size and cost of the actuator pack and kinematic certainty. For both we present our approach to accomplish them. Section II explains the mechanical design details of the proposed planar continuum robot followed by its kinematics in Section III. After these characterizations, Section IV describes the implementation details to control the motion of the arm, including simulations and experimental validation. In addition, a discussion on the mechanical limitations of the prototype are reviewed as well as noteworthy considerations when utilizing the presented designs. Finally, Section V concludes the work.

II. Mechanical Design

The novelties in design of the continuum robot concern the body structure and the actuation mechanism. Following, details of the mechanical design as well as its specifications are introduced, which are summarized in Table I.

TABLE I: Main specifications of the planar continuum robot

Feature	Value
Degrees of freedom	6 (1 per section)
Mass (arm and actuator pack)	2.4 kg
Arm dimensions	$35\times62\times940mm$
Actuator pack dimensions	$180\times100\times300mm$
Number of sections	6
Number of actuators	6 (1 per section)[1]
Number of links	30 (5 per section)
Bending capability	$\pm180°$
Section bend capability	$\pm150°$
Minimum bending radius	59mm
Actuation type	single pulley & tendons
Tendon material	0.35mm Dyneema®[2]
Bend homogenizing mechanism	Synchronizing gears

1- Without counting the one for linear movement
2- Ultra-High Molecular Weight Polyethylene

A. Body Structure

A fully articulated body with high number of rigid links is chosen as the key concept to address the requirements of kinematic certainty and high dexterity. Subsequently, in order to decrease the required actuator quantity, the number of individually actuated units is reduced. This was considered obtainable by dividing the body into groups of links, which we call sections hereafter. These design choices lead to the challenge of homogenizing the movements of the links within each section. The existing studies which have employed this base concept, employ spring elements as the homogenizing agent; e.g., works of Dong et al. [24] and Li and Du [22]. In this work, geared mechanical engagement among links is proposed as the alternative homogenizing agent.

The main parameters concerning the body of the prototype, constructed for this study, are as follows. Each individually actuated section consists of five identical links connected together via revolute joints. The robot has six of these sections connected to each other also using revolute joints forming a chain of 30 links. This enables the bounds of bending capability to $\pm180°$, limited by the characteristics of the actuator. In order to implement the intended body structure, a cable carrier with 30.5mm long links is used and the rest of the parts were assembled onto it. The sections are tendon driven and 3D-printed tendon-guides were fitted around each link to accommodate six pairs of tendons. The body and the tendon guides are depicted in Fig. 1, Fig. 2 and Fig. 3.

B. Synchronization Gears

In order to homogenize the movements of links within a section, they are engaged to one-another using gears. In Fig. 2 the mechanism of the synchronization is depicted using 2D diagrams and 3D models. For this purpose, two sector-gears are rigidly installed on top or bottom face of the links in an alternating manner. Fig. 2a shows two identical gears engaged with one another: G1 and G2. Due to the 1 to 1 ratio, when G2 rotates as much as 2θ with respect to G1, the line connecting gear centers rotates half as much. This is because the lines connecting the pitch circles' contact point and gear centers, form an isosceles triangle and an exterior angle of a triangle is equal to the sum of the opposite interior angles. As illustrated in Fig. 2b, G1 and G2 are fixed on link_0 and link_2 frames, respectively, while link_1 frame always remains in the same orientation as the line connecting G1 and G2 centers. When G2/link_2 rotates as much as 2θ with respect to G1/link_0, link_1 rotates as much as θ. Consequently G2/link_2 has rotated as much as θ with respect to link_1. This way, link_1 and link_2 movements are synchronized. In each section, the same mechanical engagement is present for all possible groups of three consecutive links, e.g. links 1,2 and 3, etc. This engagement synchronizes the movements of the last two links in each group. Overlapping engagements leads to equal relative movement of all links in a section. The last link of each section performs as base/angle reference for the subsequent section, identical to the role of link_0 in the example. The first link of each section is not engaged to any preceding link thus does not have a rear gear. Similarly, in each section, the penultimate link is not engaged to any succeeding link and does not have a front gear. We call this absence of gears a sync breaker, which enables linked sections to move independently (see Fig. 2c).

C. Spiral Pulley

The design purpose of the pulley is to perform actuation of each section with a single actuator (see Fig. 3b). Since the links are identical, calculations can be done for a pair of links then extended to the entire arm. First, the tendon length and its changes is calculated via geometry (see Fig. 3a):

$$s_0 = (l - t) \text{ and } s = s_0 cos(\theta/2), \tag{1}$$

$$s_{out} = s + w\sin(\theta/2), \tag{2}$$

$$s_{in} = s - w\sin(\theta/2), \tag{3}$$

where l, w and t are length of a link from joint to joint, width of the link from one tendon hole to the opposite and thickness of the tendon guide, respectively.

Inner and outer tendon length between two tendon guides, s_{in} and s_{out}, are calculated as a function of link rotation angle θ, and initial tendon length s_0. For clarity, s, the center distance of tendon guides, is used as an intermediate parameter. The length of the tendons running through an entire section, L, is calculated by multiplication since the movements of the links are synchronized within the section. For a section consisting of m number of links and the total bending of the section, $\phi = m\theta$, the inner and outer tendon length L_{in} and L_{out} are calculated as:

$$L_{in} = ms_{in} + mt, \tag{4}$$

$$L_{out} = ms_{out} + mt. \tag{5}$$

The amount of tendon length change at a certain bending angle

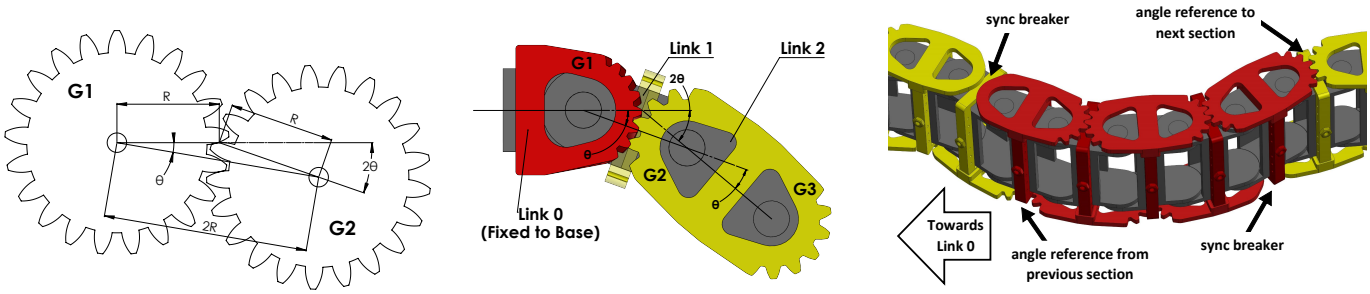

(a) Gear synchronization diagram with pitch radii of the gears R and rotation θ.

(b) Gear synchronization of the first two links.

(c) Gear engagement between links and sections implemented on top and bottom of the robot.

Fig. 2: Illustrations of the geometry principle of gear synchronization (a), synchronization of the initial two links (b) and the engagement between links and sections (c).

and their difference are:

$$\Delta L_{out} = m\left(s_0 - \left(s + w\sin(\theta/2)\right)\right) + mt, \quad (6)$$

$$\Delta L_{in} = m\left(s_0 - \left(s - w\sin(\theta/2)\right)\right) + mt, \quad (7)$$

$$\Delta L_{out} - \Delta L_{in} = 2mw\sin(\theta/2). \quad (8)$$

Consequently, for a given rotation angle, the difference between the tendon length that needs to be released to one side, and retracted from the other is bigger for wider robots. Moreover, the difference will grow as the bending angle changes toward $\pm 180°$. The difference accumulates for the the entire body of the robot and can grow large enough to raise issues. This tendon length difference can render a common cylindrical pulley that releases/retracts equal lengths of tendon on both sides, unsuitable for this job. In order to satisfy this requirement, a special pulley with a logarithmic spiral [25] profile was designed, depicted in Fig. 3b. The spiral profile effective radius is calculated as follows:

$$r = ke^{b\psi}, \quad (9)$$

where ψ is the pulley/actuator angular position and k and b are constants which were found by experiment.

The servomotor chosen for this prototype, *Dynamixel AX12-A*, has a $\pm 150°$ span and the target bending ability for the robot was selected as much as $\pm 180°$. These parameters and the calculated tendon length changes using Eq. (2) and Eq. (3) were used as inputs in finding the spiral parameters. The pulley was designed using two of these profiles back to back in a single pulley. Each of the spirals is responsible for retracting/releasing one of two tendons connected to a section. As the pulley rotates, the effective radius on one side of it increases while the opposite happens on the other side and the desired effect is achieved.

III. Kinematics

In this section, the basis and mathematical relations of actuator positions with robot parts positions are presented. Due to the nature of the proposed body structure, the robot falls into the category of constant curvature continuum robots.

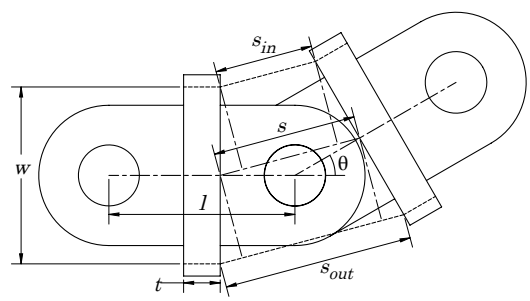

(a) Top view of two isolated links.

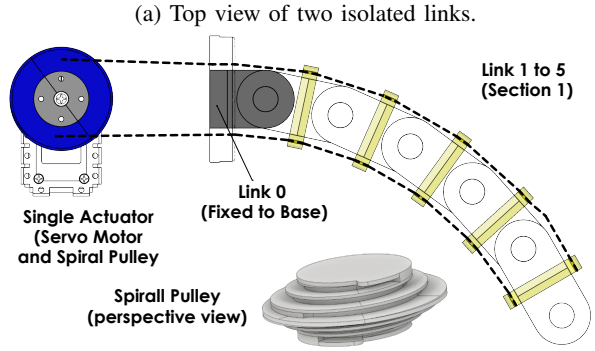

(b) Single motor with pulley (blue) to actuate one section, which contains five links (top view).

Fig. 3: Illustrations of the continuum robot design depicting individual links (a) and a tendon-actuated section (b). Note: gears are not shown for clarity and dashed lines represent the tendons.

The kinematics of these robots can be modeled using three spaces and the mappings between them [26]. The first one is the actuator space which concerns the actuator-pulley angular position, ψ, and length of tendons L_t. This space needs to be mapped to the configuration space, i.e, the bending angle of each section, ϕ. The third, the task space, defines the position and orientation of the end-effector, as well as those of the rest of the links. The configuration space needs to be mapped from/to the task space independently.

A. Actuator to Configuration Space

The calculations regarding the relation between running tendon length, L_t, and joint configuration, i.e., section bending angle ϕ, was covered in pulley design (see Section II-C). If the bending angle value for the outer tendon is considered as negative and $m = 5$, Eqs. (1) to (5) can be summarized as:

$$L_t = (l - t)\cos(\phi/10) - w\sin(\phi/10). \tag{10}$$

While the tendon length calculation is part of the actuation space mapping, it is not required in this design. The pulley is designed based on the actuator range and the target bending range of the robot. Consequently, a certain actuator-pulley position translates to a specific bending angle in the configuration space. This mapping is performed linearly as shown in Eq. 11, e.g. with actuator at sample points on half and the bounds of its range, ±75° and ±150°, the corresponding section will be at half and the bounds of the target range ±90° and ±180°. In other words, mapping the actuator space to tendon lengths and ultimately configuration space, is already done during the pulley design and is mechanically constrained.

$$\psi = \frac{\phi}{\phi_{max} - \phi_{min}}(\psi_{max} - \psi_{min}). \tag{11}$$

Actuators of further sections, have part of their tendons through preceding sections. Furthermore, change in bend angles of previous sections will impose tendon length change on the ones succeeding them. Therefore, each actuator also needs to compensate for the superposition of the bending angles of the sections preceding its corresponding section. For the desired bending angle of ith section, $\phi_{des}[i]$, the target bending angle, $\phi_{tgt}[i]$, is calculated as:

$$\phi_{tgt}[i] = \sum_{n=1}^{i} \phi_{des}[n], \tag{12}$$

where $\phi_{tgt}[i]$, the rotation of the ith section with respect to the base, is input to Eq. (11) in order to calculate the actuator position.

B. Configuration to Task Space

Since the arm consists of rigid links attached to each other via revolute joints, Modified Denavit Hartenberg (MDH) is the most straight forward approach to model the kinematics. All the moving links have the same length, $a_i = l = 30.5mm$. The type of the arm is planar and all the joints are parallel; furthermore, no link twist exists, $\alpha_i = 0$, and due to the same reason, the amount of offset can be opted as $d_i = 0$ for all the links. These assumptions simplify the transformation matrix for each of the links to:

$${}^{i-1}_{i}T = \begin{bmatrix} cos\theta_i & -sin\theta_i & 0 & l \\ sin\theta_i & cos\theta_i & 0 & 0 \\ 0 & 0 & 1 & 0 \\ 0 & 0 & 0 & 1 \end{bmatrix}, \tag{13}$$

where the link rotation, θ_i, is simply the bending angle of the corresponding section, ϕ, divided by the number of identical links forming the section. With the translations of all the links within the robot identified, the translation between the base and a certain link is calculated as the product of the translations that come before it:

$${}^{0}_{i}T = {}^{0}_{1}T\,{}^{1}_{2}T ... {}^{i-1}_{i}T. \tag{14}$$

The motion of the base (actuator-pack) results in a linear translation of each link with respect to the world frame. The position of the base , with respect to world frame, is denoted as x_0 and the translation of the base and the rest of the links are as follows:

$${}^{W}_{0}T = \begin{bmatrix} 1 & 0 & 0 & x_0 \\ 0 & 1 & 0 & 0 \\ 0 & 0 & 1 & 0 \\ 0 & 0 & 0 & 1 \end{bmatrix}, \tag{15}$$

$${}^{W}_{i}T = {}^{W}_{0}T\,{}^{0}_{i}T. \tag{16}$$

Using this translation, coordinates of a given point on the ith link's frame at ${}^{i}P = (x_p, y_p, z_p)$ can be translated to the world frame:

$${}^{W}P = {}^{W}_{i}T\,{}^{i}P. \tag{17}$$

Thus, the details of the proposed concepts, the prototype design and the kinematic modeling are covered. The process of experimenting and validating the presented theories and the details of individual steps taken accordingly, will be presented in the next section.

IV. Experiment and Validation

The proposed continuum robot design is realized as a prototype (see Fig. 4a) and it's motion capabilities is evaluated by path following experiments. The shapes and lengths of paths were selected in accordance with the robot's length and bending capabilities. The paths include arcs with radii of 100 to 150mm (See Fig. 6 and Fig. 7).

A. Continuum Robot Prototype

The continuum robot prototype is fabricated by utilizing 3D printing technology as much as possible and contains six tendon-actuated sections that have five links each. In addition, one motor in the actuator pack enables linear forward motion. All motors are Dynamixel AX12-A servos connected to a standard Desktop PC running Ubuntu Linux via a USB2DYNAMIXEL adaptor. The base position feedback is read using a KY-040 rotary encoder mechanically connected to the forward motion motor. The encoder is read using an Arduino board, which is connected to the PC via a USB cable. Motion planning was done using python code and robot control utilizes ROS for communication and interfacing.

Measurement of robot movements was done using April-Tag [27]. This package allows position measurements of specialized fiducial markers using a standard RGB camera. Furthermore, the even links of the robot, which have their gears facing up were equipped with markers such that their position can be measured by an overhead camera (see Fig. 4b). Four markers were added to the corners of the test table as measurement reference frame.

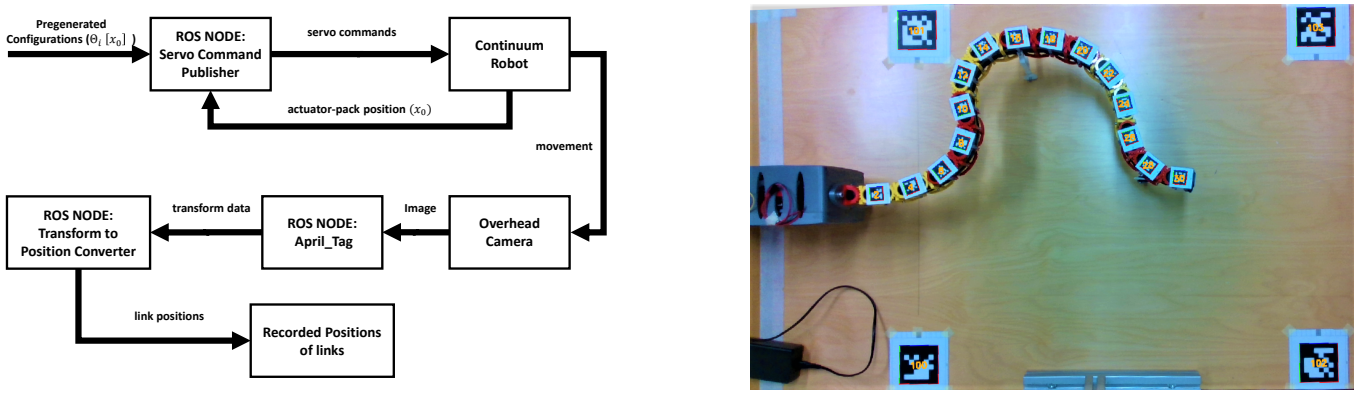

(a) Control and measurement schematics.

(b) Robot configuration tracking with AprilTag [27].

Fig. 4: Implementation (a) and experimental evaluation (b) of the tendon-driven continuum robot design.

B. Motion Planing

The robot actuator pack is installed on a rail that enables it to slide linearly. Link_0 is fixed on the actuator-pack's chassis and is not part of the actuated sections. In simulation, the coordinates of this link, $(x_0, 0, y_0)$, is the reference coordinate frame for calculation of the rest of the links' coordinates via forward kinematics (see Section III). The aim is to find a set of joint angles $\phi = (\phi_1, \phi_2, \ldots, \phi_n)$ at any given point on the path in such a way that the total distance between the continuum robot and the desired path is minimized. In each step of the simulation, Link_0 frame is moved 1mm along the X direction, i.e., x_0 is increased by 1mm. Then the optimization algorithm finds the suitable bend angles for the last two sections, ϕ_5 and ϕ_6, that best fit the predefined path. For these pioneer sections, the sum of the distances of their links' ends to the nearest point on the path are defined as the parameter which needs to be minimized:

$$P_{ij} =_i^W T \begin{bmatrix} l & 0 & 0 & 1 \end{bmatrix}^T, \tag{18}$$

$$\phi_{\mathbf{i}} = \underset{\phi_{\mathbf{i}}}{argmin} \sum_i \sum_j \|P_{ij} - Path\|, \tag{19}$$

where P_{ij} is the end point of the jth link in i^{th} section, with $i \in \{5, 6\}$ and $j \in \{1, 2, \ldots, 5\}$. Function *minimize* from *scipy.optimize* package [28] with *Powell* method [29] was used for the minimization task. The pseudo code that summarizes the process is shown in Algorithm 1.

At each iteration, the bend angles from the previous step are fed to the algorithm as the initial conditions. The rest of the sections repeat the movements of the pioneers when they are in their relative positions. The even and odd numbered ones copy the movements of the 6th and 5th sections, respectively. The algorithm continues until the length of the rail is covered and the bend angles of all six sections, and consequently their actuator angular positions, are known for all the steps. Fig. 6 depicts the resulting body shape at three locations on Path-2 and Fig. 7 illustrates the robot's planned shape on paths 1, 3 and 4 when the slider has moved +750mm forward.

Algorithm 1: Finding the robot joint configurations for a certain path

Parameters:
- x_0: link_0 position
- $\phi_{\mathbf{i}}[\mathbf{x}]$: configuration of ith section
- L_s: single section length
- L_R: rail length
- $\mathbf{P_{ij}}$: j^{th} link of ith section pose

Input : Path (array of coordinate vectors)
Output : $\phi_i[x]$ ($i \in \{1, \ldots, 6\}$, $x \in \{0, \ldots, L_R\}$)

```
x_0 ← 0
φ_{5,6}[x_0] ⇐ 0
while x_0 < L_R do
    for i=1 to 4 do
        x_i ← x_0 + 2L_s
        φ_i[x_i] ← φ_{i+2}[x_0]
    end
    x_0 ← x_0 + 1                    (base moves 1mm forward)
    φ_{5,6}[x_0] ← argmin_{φ_{5,6}} Σ_i Σ_j ||P_ij − Path||,
    P_ij ← FK(φ_i[x_0])              (Forward Kinematics)
end
```

C. Validation

The pregenerated configurations for each path from the motion planning algorithm were used to control the actual robot. As shown in Fig. 4a, the control node receives the position of Link_0 (actuator-pack) as feedback and selects the proper set of pregenerated section configurations, ϕ_i accordingly. Subsequently, the servo motor commands, ψ_i are calculated using Eq. (11) and Eq. (12) and sent to the robot. While motors responsible for moving the arm have an internal feedback ensuring the command execution, there is no direct feedback from the arm body shape.

In order to compare the achieved positions with the simulations, the deviations of simulated and actual positions from

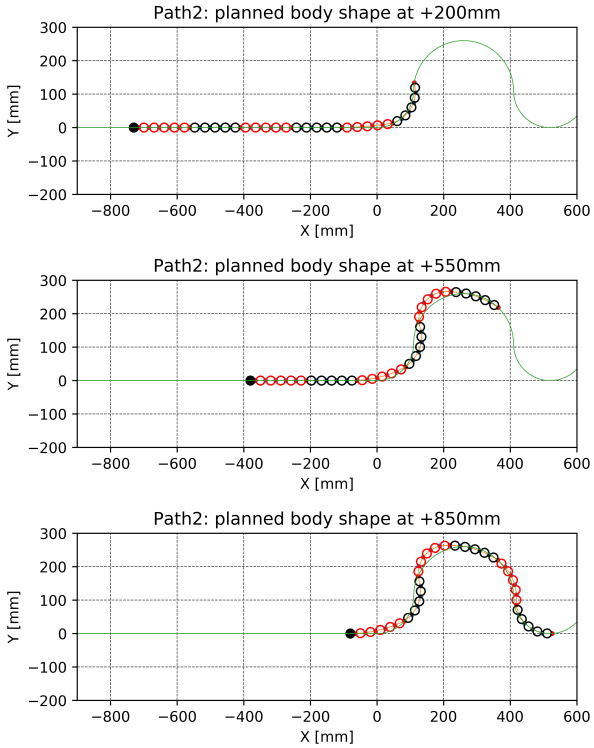

Fig. 6: Simulated robot on Path-2 (light-green) when base is at +200mm, +550mm and +850mm

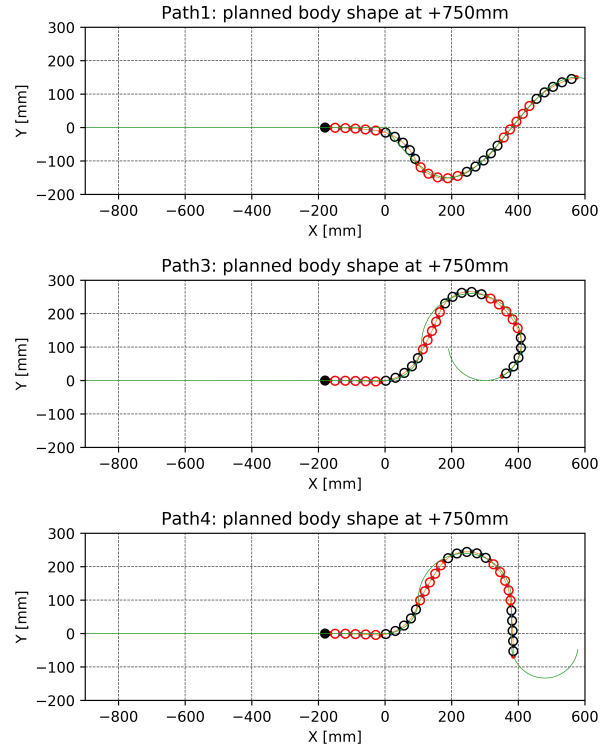

Fig. 7: Simulated robot on Path-1, Path-3 and Path-4 (light-green) when base is at +750mm

the intended paths were calculated. The maximum deviation is less than 40mm in simulation and less than 60mm in real experiments, for all the paths. Fig. 8 summarizes the deviation of simulated (a) and actual positions (b) from intended paths for even links. Each bar shows the average deviations of a link from its intended positions through the entire path. The vertical line in the middle of the bar shows the standard deviation for the corresponding data set. The relatively small differences observed in these two plots illustrates the conformity of simulation and real experiments.

D. Discussion

While the prototyping approaches explained in this section served their purposes, they caused a number of issues that needed addressing. The cable carrier has a rectangular cross-section which makes it susceptible to torsional strain and twist deformation. Placement of the gears on top and bottom of the profile exerts counteracting lateral forces which result in skewing each section and exacerbates the deforming issue. Moreover, the 3D printed material flexes under the weight of the robot and causes excessive deformation along its length. These issues were partly addressed by adding wheels to the first link of the fourth section and the last link of the robot. They partly support the weight of the robot in order to minimize the deformation. While these wheels cannot exist in a working continuum robot, they do not pose any conflict with the proof of concept purpose of this work.

V. Conclusion

This work proposes two novelties in design of continuum robots, i.e., body structure and actuation mechanism, and reports results on a developed prototype. The novel body structure introduces the concept of sections formed by articulated links, which are synchronized by gears. It is presented as an alternative to existing approaches, such as flexible sections and independently actuated articulated links. The proposed actuation method utilizes a double spiral pulley to actuate each section of the arm with a single actuator. In addition, due to the absence of spring elements, as compared to the existing methods, the torque requirement is lower, thus the size of the needed actuators is smaller. Both contributions lead to a reduction in weight, volume and cost of the actuator pack needed for planar continuum robots. The novelties were put to test by a prototype that consists of a six section planar continuum robot, which was evaluated by path following experiments. Results demonstrate that the deviation from desired and executed path stays under 40 mm and 60 mm, for a simulated and real robot, respectively.

Acknowledgements

This work was partly funded by the Engineering Physics and Detector Technologies department of CERN and by the Technology Programme of the Helsinki Institute of Physics (project; ROBOT). We want to particularly thank Mr. Corrado Gargiulo, Mr. Luca Rosario Buonocore and Miss. Elisa Laudi, who greatly helped sourcing the components.

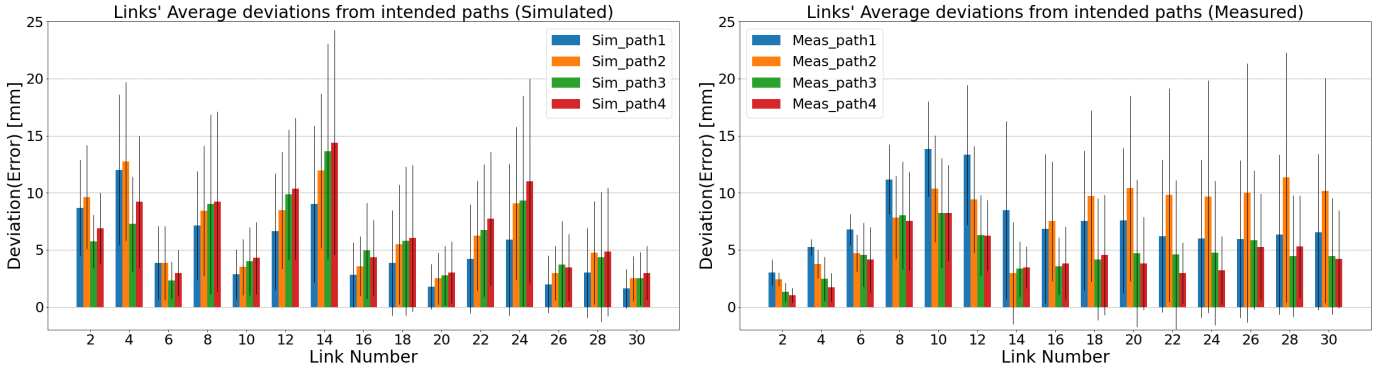

(a) (b)

Fig. 8: Summary of deviations from the paths by the simulated (a) and actual robot (b). Colored bars and the vertical lines indicate the average and standard deviation of each data set respectively.

REFERENCES

[1] H. Yang, B. Wu, X. Liu, and K. Xu, "A closed-loop controller for a continuum surgical manipulator based on a specially designed wrist marker and stereo tracking," in *IEEE/ASME International Conference on Advanced Intelligent Mechatronics (AIM)*, 2020, pp. 335–340.

[2] B. Liu, A. Zhang, J. Liu, Z. Han, and T. Xie, "Design and evaluation of a novel rotatable one-element snake bone for NOTES," *Journal of Medical Devices*, vol. 12, no. 2, 2018.

[3] A. Orekhov, C. Abah, and N. Simaan, "Snake-like robots for minimally invasive, single-port, and intraluminal surgeries," *The Enciclopedia of Medical Robotics. World Scientific*, pp. 203–243, 2018.

[4] J. Burgner-Kahrs, D. C. Rucker, and H. Choset, "Continuum robots for medical applications: A survey," *IEEE Transactions on Robotics*, vol. 31, no. 6, pp. 1261–1280, 2015.

[5] Y. Chen, J. Liang, and I. W. Hunter, "Modular continuum robotic endoscope design and path planning," in *IEEE International Conference on Robotics and Automation (ICRA)*, 2014, pp. 5393–5400.

[6] D. B. Roppenecker, L. Schuster, J. A. Coy, M. F. Traeger, K. Entsfellner, and T. C. Lueth, "Modular body of the multi arm snake-like robot," in *IEEE International Conference on Robotics and Biomimetics (ROBIO)*, 2014, pp. 374–379.

[7] N. Simaan, K. Xu, W. Wei, A. Kapoor, P. Kazanzides, R. Taylor, and P. Flint, "Design and integration of a telerobotic system for minimally invasive surgery of the throat," *The International journal of robotics research*, vol. 28, no. 9, pp. 1134–1153, 2009.

[8] L. Angrisani, S. Grazioso, G. D. Gironimo, D. Panariello, and A. Tedesco, "On the use of soft continuum robots for remote measurement tasks in constrained environments: A brief overview of applications," in *IEEE International Symposium on Measurements and Networking (M&N)*, 2019, pp. 1–5.

[9] M. Wang, D. Palmer, X. Dong, D. Alatorre, D. Axinte, and A. Norton, "Design and development of a slender dual-structure continuum robot for in-situ aeroengine repair," in *IEEE/RSJ International Conference on Intelligent Robots and Systems (IROS)*, 2018, pp. 5648–5653.

[10] X. Dong *et al.*, "Development of a slender continuum robotic system for on-wing inspection/repair of gas turbine engines," *Robotics and Computer-Integrated Manufacturing*, vol. 44, pp. 218–229, 2017.

[11] Y. Wang, F. Ju, Y. Cao, Y. Yun, Y. Wang, D. Bai, and B. Chen, "An aero-engine inspection continuum robot with tactile sensor based on EIT for exploration and navigation in unknown environment," in *IEEE/ASME International Conference on Advanced Intelligent Mechatronics (AIM)*, 2019, pp. 1157–1162.

[12] R. Buckingham *et al.*, "Snake-arm robots: a new approach to aircraft assembly," SAE Technical Paper, Tech. Rep. No. 2007-01-3870, 2007.

[13] C. G. Frazelle, A. Kapadia, and I. Walker, "Developing a kinematically similar master device for extensible continuum robot manipulators," *ASME Journal of Mechanisms and Robotics*, vol. 10, no. 2, 2018.

[14] P. S. Gonthina, M. B. Wooten, I. S. Godage, and I. D. Walker, "Mechanics for tendon actuated multisection continuum arms," in *IEEE International Conference on Robotics and Automation (ICRA)*, 2020, pp. 3896–3902.

[15] W. McMahan *et al.*, "Field trials and testing of the octarm continuum manipulator," in *IEEE International Conference on Robotics and Automation (ICRA)*, 2006, pp. 2336–2341.

[16] T. Mahl, A. Hildebrandt, and O. Sawodny, "A variable curvature continuum kinematics for kinematic control of the bionic handling assistant," *IEEE Transactions on Robotics*, vol. 30, no. 4, pp. 935–949, 2014.

[17] M. Cianchetti, T. Ranzani, G. Gerboni, I. De Falco, C. Laschi, and A. Menciassi, "STIFF-FLOP surgical manipulator: Mechanical design and experimental characterization of the single module," in *IEEE/RSJ International Conference on Intelligent Robots and Systems (IROS)*, 2013, pp. 3576–3581.

[18] A. Shiva *et al.*, "Tendon-based stiffening for a pneumatically actuated soft manipulator," *IEEE Robotics and Automation Letters*, vol. 1, no. 2, pp. 632–637, 2016.

[19] Y. J. Kim, S. Cheng, S. Kim, and K. Iagnemma, "Design of a tubular snake-like manipulator with stiffening capability by layer jamming," in *IEEE/RSJ International Conference on Intelligent Robots and Systems (IROS)*, 2012, pp. 4251–4256.

[20] Y. Hu, L. Zhang, W. Li, and G. Z. Yang, "Design and fabrication of a 3-D printed metallic flexible joint for snake-like surgical robot," *IEEE Robotics and Automation Letters*, vol. 4, no. 2, pp. 1557–1563, 2019.

[21] Z. Du, W. Yang, and W. Dong, "Kinematics modeling of a notched continuum manipulator," *ASME Journal of Mechanisms and Robotics*, vol. 7, no. 4, 2015.

[22] Z. Li and R. Du, "Design and analysis of a bio-inspired wire-driven multi-section flexible robot," *International Journal of Advanced Robotic Systems*, vol. 10, no. 4, p. 209, 2013.

[23] P. Qi, C. Qiu, H. Liu, J. S. Dai, L. Seneviratne, and K. Althoefer, "A novel continuum-style robot with multilayer compliant modules," in *IEEE/RSJ International Conference on Intelligent Robots and Systems (IROS)*, 2014, pp. 3175–3180.

[24] X. Dong, M. Raffles, S. Cobos-Guzman, D. Axinte, and J. Kell, "A novel continuum robot using twin-pivot compliant joints: design, modeling, and validation," *ASME Journal of Mechanisms and Robotics*, vol. 8, no. 2, 2015.

[25] E. Weisstein, ""logarithmic spiral." from mathworld, a wolfram web resource," https://mathworld.wolfram.com/LogarithmicSpiral.html, accessed: 2020-04-03.

[26] R. J. Webster and B. A. Jones, "Design and kinematic modeling of constant curvature continuum robots: A review," *International Journal of Robotics Research*, vol. 29, no. 13, pp. 1661–1683, 2010.

[27] J. Wang and E. Olson, "AprilTag 2: Efficient and robust fiducial detection," in *IEEE/RSJ International Conference on Intelligent Robots and Systems (IROS)*, 2016, pp. 4193–4198.

[28] P. Virtanen *et al.*, "SciPy 1.0: Fundamental algorithms for scientific computing in Python," *Nature Methods*, vol. 17, pp. 261–272, 2020.

[29] M. J. D. Powell, "An efficient method for finding the minimum of a function of several variables without calculating derivatives," *The Computer Journal*, vol. 7, no. 2, p. 155, 1964.